Real time, confocal imaging of Ca^{2+} waves in arterially perfused rat hearts

Andreas P. Baader, Lorenz Büchler, Lilly Bircher-Lehmann, André G. Kléber*

University of Bern, Department of Physiology, Bühlplatz 5, 3012 Bern, Switzerland

Abstract

Objective: The aim of this study was to characterize the spatio-temporal dynamics of slow Ca^{2+} waves (SCW's) with cellular resolution in the arterially-perfused rat heart. **Methods:** Wister rat hearts were Langendorff-perfused with Tyrode solution containing bovine-albumine and Dextran. The heart was loaded with the Ca^{2+} sensitive dye Fluo-3 AM. Intracellular fluorescence changes reflecting changes in $[Ca^{2+}]_i$ were recorded from subepicardial tissue layers using a slit hole confocal microscope with an image intensified video camera system at image rates of up to 50/s. **Results:** SCW's appeared spontaneously during cardiac rest or after trains of electrical stimuli. They were initiated preferentially in the center third of the cell and propagated to the cell borders, suggesting a relation between the cell nucleus and wave initiation. They were suppressed by Ca^{2+} transients and their probability of occurrence increased with the Ca^{2+} resting level. Propagation velocity within myocytes (40 to 180 μm/s) decreased with the resting Ca^{2+} level. Intercellular propagation was mostly confined to two or three cells and occurred bi-directionally. Intercellular unidirectional conduction block and facilitation of SCW's was occasionally observed. On average 10 to 20% of cells showed non-synchronized simultaneous SCW's within a given area in the myocardium. **Conclusions:** SCW's occurring at increased levels of $[Ca^{2+}]_i$ in normoxic or ischemic conditions are mostly confined to two or three cells in the ventricular myocardium. Spatio-temporal summation of changes in membrane potential caused by individual SCW's may underlie the generation of triggered electrical ectopic impulses. © 2001 Published by Elsevier Science B.V.

Keywords: Arrhythmia (mechanisms), Calcium (cellular), Conduction system, Signal transduction

1. Introduction

Changes of cytoplasmic $[Ca^{2+}]$ during the cardiac cycle are characterized by a complex interplay of Ca^{2+} entering from the extracellular space, Ca^{2+} released from the intracellular stores, Ca^{2+} pumped into intracellular stores, and Ca^{2+} transferred from the cytoplasm to the extracellular space. Since some of these processes induce changes in transmembrane voltage by affecting transmembrane ionic channels and transporters, fluctuations in intracellular Ca^{2+} can contribute to repetitive depolarizations, and consequently, to arrhythmias. Thus, oscillations of transmembrane potential have been reported as a consequence of

reactivation of L-type Ca^{2+} currents during a prolonged duration of the action potential plateau (early afterdepolarizations, EAD's) and as the result of electrogenic extrusion of Ca^{2+} via the Na/Ca exchanger after repolarization of the action potential (delayed afterdepolarizations, DAD's). Additionally, Ca^{2+} bound to Troponin C can induce Ca^{2+} transients in the case of rapid force changes [1]. While these events necessitate coordinated action of many myocytes to produce a source for electrical excitation, Ca^{2+} changes in the cytoplasm have been reported to occur in discrete entities that appear to relate to the special compartment structure of the SR. The overall increase of cytoplasmic Ca^{2+} during a contraction cycle then results from the independent and discrete summation of local Ca^{2+} releases (sparks). When reaching a critical cellular cytoplasmic $[Ca^{2+}]$ of about 500 nM [2], local sparks can

*Corresponding author. Tel.: +41-31-631-8740; fax: +41-31-631-8785.

E-mail addresses: baader@pyl.unibe.ch (A.P. Baader), kleber@pyl.unibe.ch (A.G. Kléber).

Time for primary review 29 days.

turn into propagating waves. Analysis of Ca^{2+} waves, and especially their propagation and co-ordination within and among cells is important for our understanding of initiation of arrhythmias. It was not until recently that the first studies described Ca^{2+} waves in multicellular cardiac muscle preparations [3–6]. In trabeculae muscles, propagating waves were found to originate from mechanically damaged muscle fiber regions [7–9]. These waves could travel into undamaged myocardium areas to cause triggered propagated contractions (TCP's) of the sarcomeres. But the probability that this intercellular propagation occurred was found to be rather low [10]. Spontaneous Ca^{2+} oscillations were also reported in whole rat hearts. Minamikawa et al. [5] described multifocal waves, the activity of which increased with Ca^{2+} overload and which had propagation velocities of 60–100 $\mu m/s$. Hama et al. [11] gave a qualitative description of wave propagation in ventricular myocytes. Most recently, the interactions between Ca^{2+} waves and transients and the intra- and intercellular propagation characteristics of Ca^{2+} waves were studied in perfused rat hearts (Kaneko et al. [12]) and in Purkinje cells [13].

In the present study, we investigated the occurrence of slow Ca^{2+} waves (SCW's) in arterially-perfused whole rat hearts in dependence of different cytosolic Ca^{2+}. The aim was to provide a detailed intracellular characterization of the temporal and spatial dynamics of SCW's. A slit hole confocal imaging system was used for real time acquisition of intracellular Ca^{2+} changes that had both a high sensitivity and a high speed of up to one frame every 20 ms. This allowed us to investigate Ca^{2+} fluctuations in

myocytes of the whole heart over a relatively large area of cardiac tissue.

2. Methods

The investigation conforms with the *Guide for the Care and Use of Laboratory Animals* published by the US National Institutes of Health (NIH Publication no. 85-23, revised 1996).

2.1. Langendorff hearts and experimental setup

After anesthesia 3–6-day-old Wister rats were decapitated. The excised hearts (weight: 40–60 mg) were brought to a Langendorff-chamber. Time from excision to cannulation was less than 5 min. In the perfusion chamber the heart was equilibrated with perfusion solution containing Tyrode solution with 1.8 mM Ca^{2+}, bovine-albumine (2 g/l) and Dextran (40 g/l) [14]. The preparations were stimulated at 2 Hz by means of two platinum wires (20 μm diameter) inserted into the ventricular myocardium. Temperature inside the chamber was set to 35–37°C. A subsequent equilibration period of 30 min allowed the heart to recover and to adjust constant pressure and temperature conditions in the chamber.

The perfusion system has been described previously in detail [15]. In brief, it consisted of a roller pump, a silicone membrane gas exchanger and a Perspex recording chamber (Fig. 1). The roller pump generated a sustained perfusion pressure of 40 to 55 mm Hg. N_2-, CO_2- and O_2-levels in
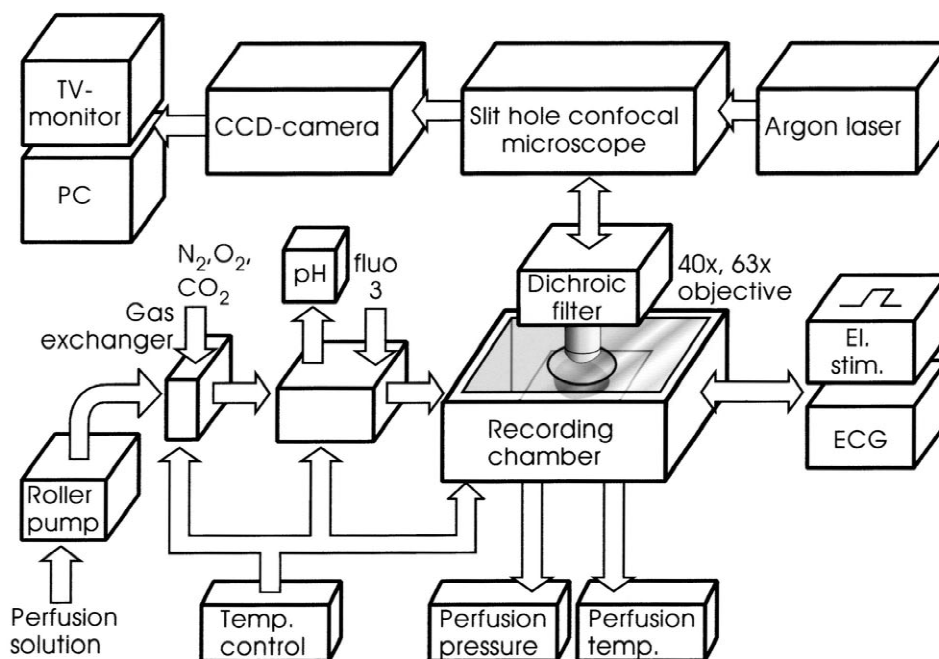

Fig. 1. Experimental setup for the recording of myocardial Ca^{2+} fluctuations in rat hearts. The Langendorff-perfused heart is positioned left ventricle up in a sealed recording chamber under constant temperature and full H_2O saturation conditions. It is paced electrically (El. Stim.) by means of platinum wires inserted into the left ventricle. The Ca^{2+} sensitive dye Fluo-3 AM is loaded into the myocardium through the perfusion system. Fluorescence excitation of Fluo-3 dye is provided by a 488-nm Argon laser and recorded through a slit hole confocal microscope by an image-intensified video camera system.

the solution and in the surrounding H_2O-saturated atmosphere of the chamber were adjusted to maintain an oxygen concentration of $\geq 99\%$ and a pH of 7.4. In the perfusion chamber, the heart was mounted on a wax platform with the left ventricle up. A 150 μm thick glass cover slip was mounted in a 30 mm wide circular opening in the lid, directly above the heart gently depressing the myocardial surface. It sealed the recording chamber completely and prevented excessive movements.

Neonatal rat hearts were chosen because loading of the myocytes with Ca^{2+}-sensitive dyes via arterial perfusion was faster and provided more homogenous staining than adult rat hearts. Neonatal hearts differ from adult myocardium by a somewhat different cellular structure with a smaller density and a less regular organization of cells. Although the distribution of some membrane channels was also found to be different [16,17], the major ion channels and gap junctions present in adult hearts are fully expressed, and neonatal myocytes show a stable intracellular Ca^{2+} concentration between P1 (postnatal day 1) and P7 [17]. The hearts beat in normal sinus rhythm and can be overdriven by ventricular stimulation.

As another morphological characteristic neonatal rat myocytes are predominantly mononucleic while adult myocytes have two nuclei per cell. We stained neonatal ventricles with eosine and glutaraldehyde, and found virtually no binucleate cells at P3 and a very low proportion of binucleate myocytes in P6-ventricles, the oldest postnatal state used in our experiments. We also found that all nuclei were consistently located within the center third portion of the cells. These results are in agreement with previous morphometric studies [18], which report 2.94, 15.16 and 50.6% binucleate myocytes in left ventricular myocardium of P1, P5 and P11 postnatal rat hearts, respectively.

2.2. Confocal Ca^{2+} imaging

The whole chamber assembly was positioned on a movable stage under an upright slit detector confocal microscope (Meridian Insight). Imaging was performed at 40× (water immersion, C-Apochromat, NA1.2, Zeiss) and 63× (oil immersion, Plan-Neofluar, NA1.25, Zeiss) magnification. With the 40× objective confocal imaging provided a sharp image in a depth of ± 1.5 μm around the focal plane. A CCD video camera with GEN II – image intensifier (MXRI, Adimex Image Systems) recorded interlaced 8 bit images at a frequency of 25 frames/s and a size of 604×575 pixels. By de-interlacing the video sequences off-line frame rates of 50 frames/s could be achieved. Video images were acquired with a Matrox Pulsar grabbing board on a Pentium II computer at a transfer rate of ≤ 60 MB/s. Images could be acquired down to a depth of 150 μm from the surface of the myocardium before blurring occurred. A laser power of 80% of the maximum output (nominally 500 mW) was used to produce fluorescence signals. The gain of the

image intensifier was routinely adjusted at the beginning of each experiment so that electrically induced Ca^{2+}-transient-peaks produced non-saturated pixel values. During image acquisition the laser beam continuously illuminated recording the preparation. Interlaced video images were acquired in series of up to 80 frames using the video grabbing board and/or were recorded continuously on videotape. During these (up to 3.2 s) recording periods no bleaching of signals were observed. With recording times ≥ 5 s bleaching produced a gradual reduction in fluorescence intensity (see Fig. 2). Largest recorded regions of interest (ROI's) were 150–250×235 μm with the 40× objective and 100–150×150 μm with the 63× objective, and depended on the deflection amplitude of the oscillating mirror in the confocal microscope. From these images, sub-ROI's were off-line selected for analysis using NIH Image software. Ca^{2+}-induced fluorescence changes were calculated from image series. Background fluorescence (F_{back}) was determined from a 144-pixel-area within the recording region where no myocyte was discerned. Non-ratiometric estimation of Ca^{2+} changes was expressed either as arbitrary units (a.u.), derived directly from the 8-bit gray level contents of the images after subtraction of the background fluorescence, or as ratio with $F/F_0 = (F_{max}F_{back})/(F_{base} - F_{back})$ or $\Delta F/F = (F_{max}F_{base})/(F_{base}F_{back})$ [19]. F_{max} is the peak fluorescence of the Ca^{2+}-mediated signal and F_{base} represents the fluorescence level of the myocyte during rest. For the calculation of the velocities of individual Ca^{2+} waves a look-up table (LUT) of 12 colours representing levels of F/F_0 was applied. Conduction velocity was evaluated from the spatial progression of the intensity values in the steepest part of the wave front. Cell borders were determined from off-line averaged series of images.

2.3. Experimental procedure

During loading of the myocardium with Ca^{2+}-sensitive fluorescent dye (fluo 3-AM, Teflabs, 4 μmoles/l in 20 ml perfusate), the temperature of the chamber and of the perfusion solution was lowered to 7–10°C. Depending on the flow rate cold loading lasted for 30 to 40 min. Afterwards, the hearts were perfused with dye-free solution at 35–37°C. In most experiments it was possible to obtain mechanically stable recordings. In 14 of the 29 experiments excessive contractions interfered with the optical recordings. In these cases 2,3-butanedione monoxime (BDM, 20 mM) was added to the solution to minimize contractions.

SCW's appeared spontaneously in electrically quiescent preparations or they were induced after bursts of rapid stimuli. These trains modified cytosolic free [Ca^{2+}]. A gradual increase of cytosolic resting [Ca^{2+}] levels was also observed during extended recording periods of up to 1 h. Therefore, this method was used to investigate the relationship between SCW's and [Ca^{2+}]$_i$. In all measurements,
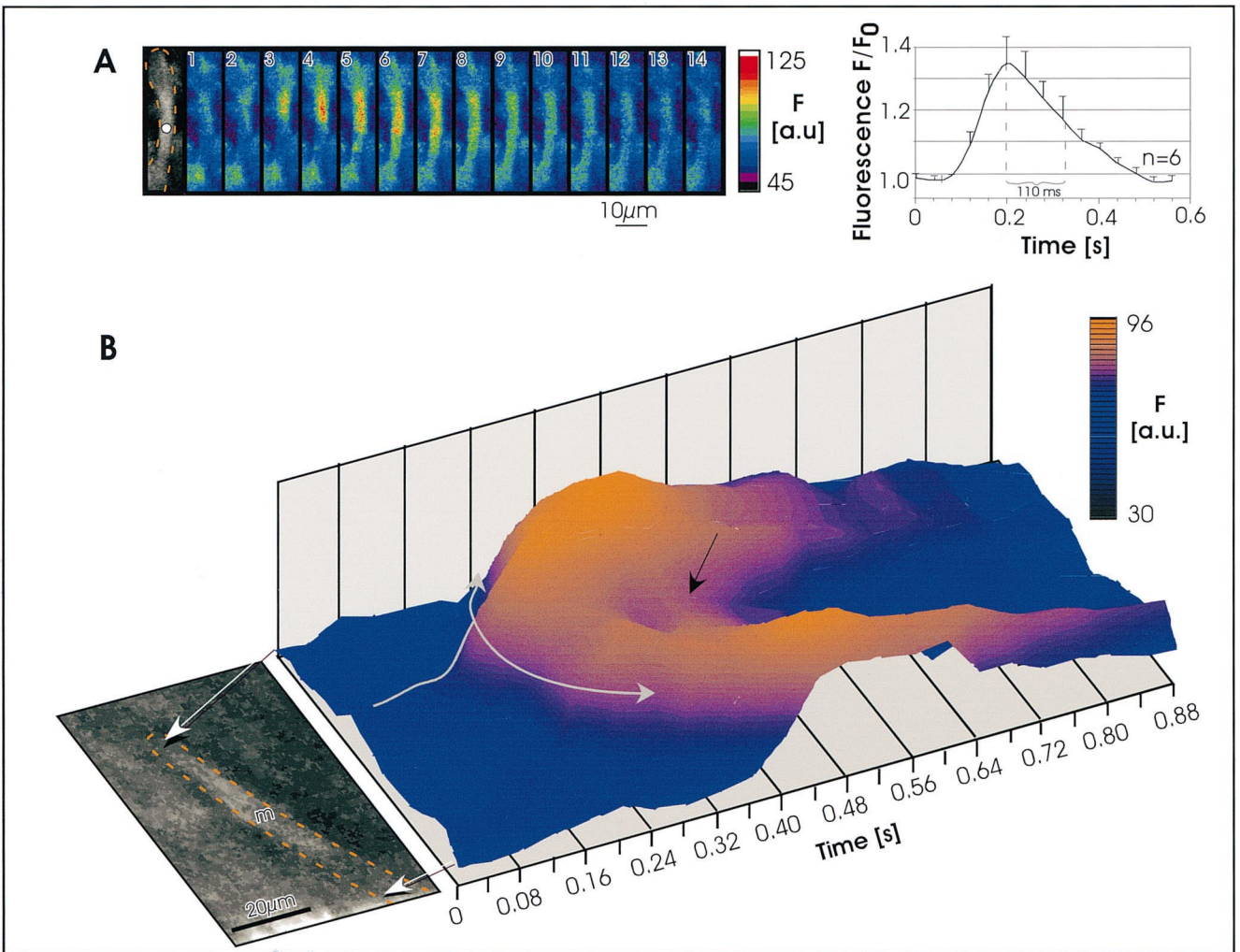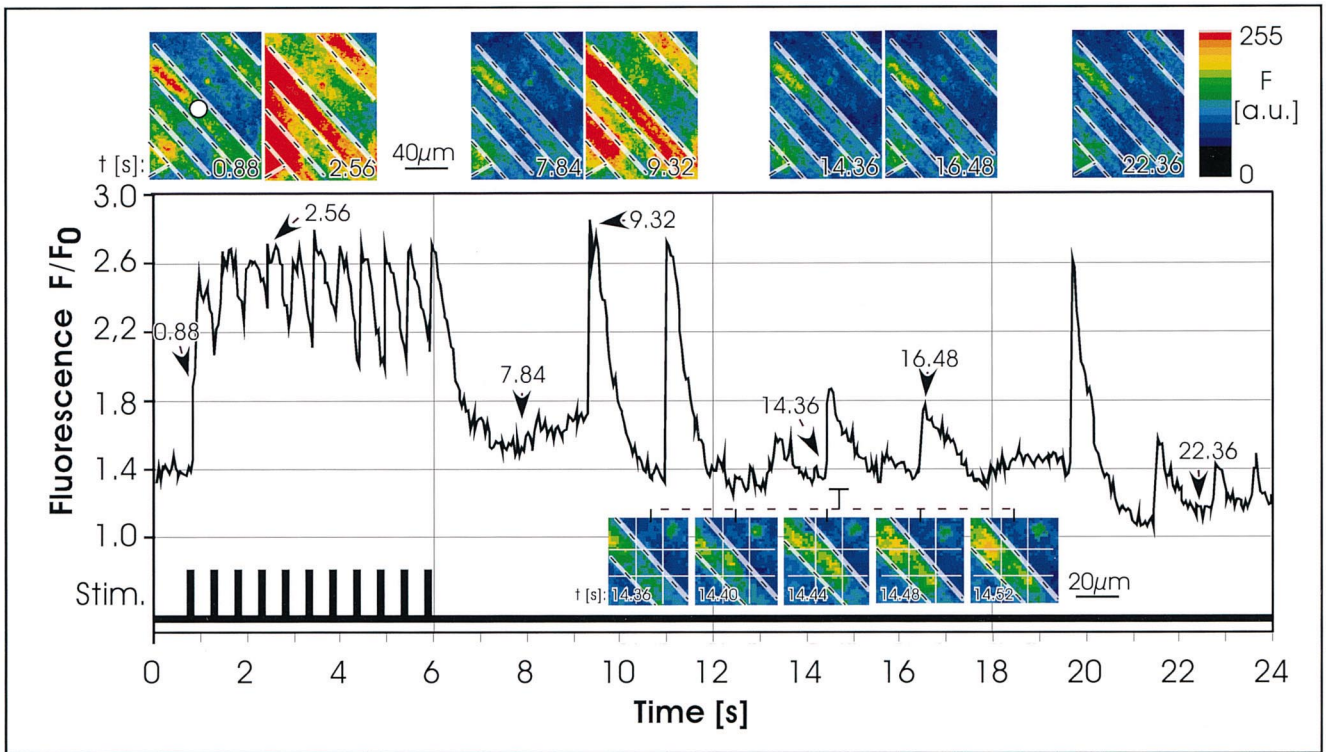
when SCW's were measured rapid Ca^{2+} transients reflecting the cytosolic Ca^{2+} increase during normal electrical excitation were observed. This excluded electrical conduction block due to Ca^{2+}-induced cell-to-cell uncoupling during the occurrence of SCW's.

3. Results

3.1. Calcium signals in ventricular myocytes

Two distinct types of Ca^{2+} fluctuations were observed: (1) Ca^{2+} transients that appeared synchronized across the whole muscle tissue at the available time resolution and that followed electrical excitation, and (2) local waves, which propagated within and/or between myocytes (slow Ca^{2+} waves, SCW's). In Fig. 2 fluorescence changes in a small cardiac area from a typical experiment are depicted. The pseudo color images of the upper panel show three myocytes in the focal plane labeled as green to red areas and confined by dashed lines. They are separated by cells not fully in the focal plane and by extracellular clefts (blue areas). Mean intensity changes (F/F_0) were recorded from a circular 144-pixel-ROI (18 μm diameter, white circle in the upper left image). Within the first 6 s of this recording, the heart was burst-paced at 2.3 Hz. Ca^{2+} transients appeared synchronized over the entire muscle tissue. The recovery time course (the time at 50% maximum amplitude) was 210 ± 85 ms ($n=95$), and longer than the inter-stimulus interval, and consequently, the Ca^{2+} level remained elevated throughout the stimulation period. After termination of the electrical burst, resting Ca^{2+} level decreased but remained still higher than before burst stimulation. This gave raise to a first and second spontaneous Ca^{2+} transient after $t=9.3$ and 11.2 s. At $t=13$ s an SCW developed, followed by additional SCW's and occasional Ca^{2+} transients. During this long period of laser stimulation (24 s) the average baseline fluorescence gradually decreased as a consequence of dye bleaching.

Spontaneous SCW's in the myocytes appeared as local spots before their wave fronts propagated to the periphery (Fig. 3A). The values of the temporal dynamics of the wave in this figure were acquired from the round ROI indicated by the white circle. Peak intensity values of $F/F_0=1.2$ to 1.5 were reached after 100–200 ms and decayed during the subsequent 400 ms with a half decay time of 110 ms. These intensities were typical for the majority of SCW's observed under normoxic conditions (see also Fig. 2). The mean propagation velocity of this wave was 130 μm/s. A detailed spatio-temporal distribution of such a wave *within* a myocyte is shown in Fig. 3B. The first phase started with a circumscribed rise in Ca^{2+} near the center of the cell. This local spot increased in size for about 40 ms until it reached a certain concentration level. In a second phase, two wave fronts (gray arrow lines in Fig. 3B) emerged from this central site to the periphery while further increasing in intensity. When the two centrifugal waves were at their highest intensity, the Ca^{2+} concentration at the site of origin of the wave began to decrease. The third phase was characterized by a general Ca^{2+} decrease throughout the whole cell. Although in this example propagation of Ca^{2+} into neighboring cells at the same focal plane was not observed, it can not be ruled out that Ca^{2+} spread occurred into cell layers above or below. A secondary small central Ca^{2+} increase was visible after some 200 ms at the site of origin of the wave (black arrow), which however did not develop into a second wave. While in our experiments most of the observed SCW's (79.1%, 43 observations) originated in or near the center third of the cell, others could also start in the cell periphery (see also Ref. [10]).

3.2. Dynamics common to slow Ca^{2+} waves

As shown in Fig. 2, SCW's always appeared in periods between Ca^{2+} transients, and preferentially, after multiple transients induced by burst pacing. Ca^{2+} transients suppressed ongoing slow wave activity completely, no matter whether they had been electrically induced or occurred spontaneously. As illustrated in Fig. 4A, the delay T_W between a transient and the first SCW in a given myocyte depended on the amplitude of the preceding Ca^{2+} transient. The higher its amplitude the longer was the time interval T_W until the first slow wave was observed (Fig. 4B). The regression of measurements in 27 myocytes from 15 experiments was $R=0.70$. In general, resting Ca^{2+}

Fig. 2. Electrically induced and spontaneous Ca^{2+} fluctuations in myocytes of a perfused P6-rat-heart. Fluorescence changes (F/F_0) were calculated from video images taken every 40 ms during 25 s. Selected pseudo color images are shown at the times indicated. Dashed lines surround three myocytes in the focal plane. Measurements were taken from one cell at a 144-pixel-ROI (white circle in upper left image). During the first 6 s the preparation was stimulated electrically at 2 Hz (see stimulation pattern in bottom trace), resulting in brief Ca^{2+} transients. After termination of the electrical stimulation two spontaneous Ca^{2+} transients (at $t=9.3$ and 11.2 s) appeared, followed by a series of lower amplitude Ca^{2+} waves and another transient. The course of one such slow Ca^{2+} wave is shown in detail in the lower continuous image sequence. No BDM was used in this experiment.

Fig. 3. Intracellular propagation characteristics of single slow Ca^{2+} waves. (A) Propagation of a wave within a single ventricular myocyte (outlined by the orange dotted line). Pseudo color images of 14 consecutive frames, every 40 ms. The local fluorescence changes in this cell were measured at the point indicated by a white circle and their average intensity values during six waves are plotted in the graph below. (B) Typical phases of wave propagation within another myocyte (m, outlined by the orange dotted line). Intensity changes were measured simultaneously every 20 ms at 15 non-overlapping 174-pixel-ROI's along the longitudinal midline of the cell. A central local Ca^{2+} increase is followed by a Ca^{2+} spread towards the peripheral membrane boundaries, a central decrease and finally a peripheral decrease of Ca^{2+}. No BDM was used in this recording.
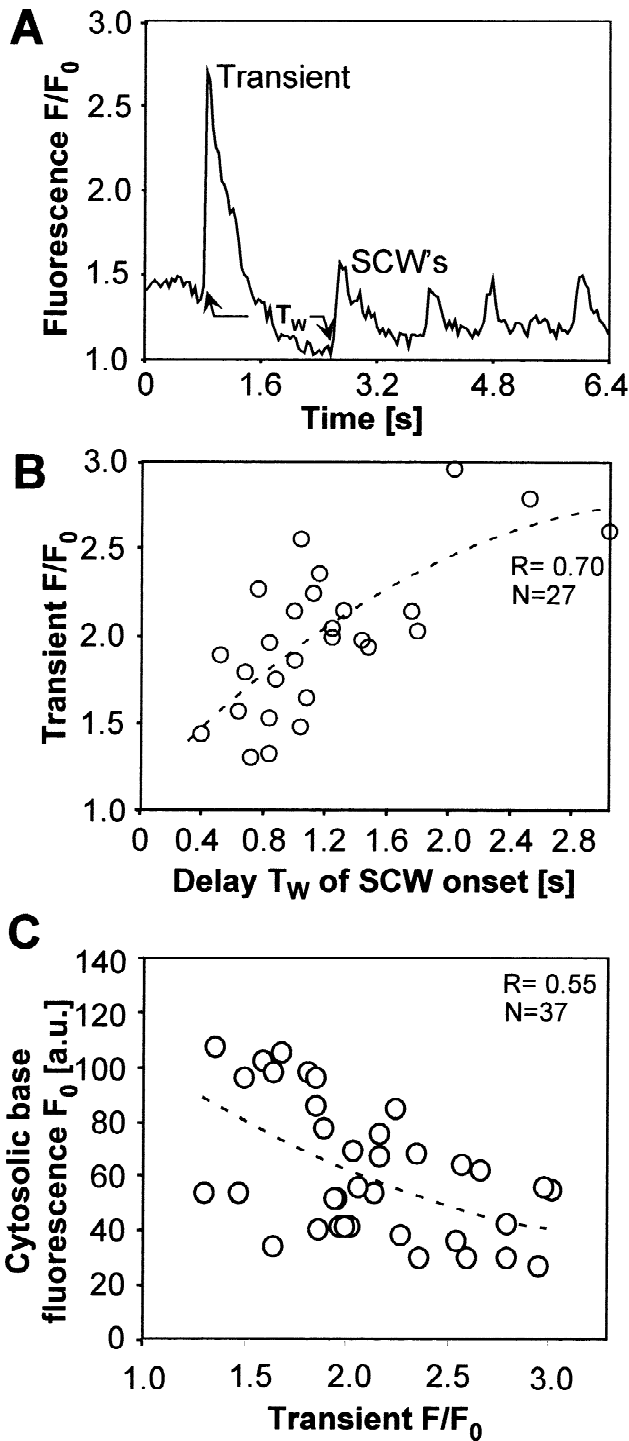
Fig. 4. The amplitude of Ca^{2+} transients affects the onset of subsequent slow Ca^{2+} waves and changes with the cytosolic Ca^{2+} load. (A) Example of a single Ca^{2+} transient followed by slow local waves. Arrows indicate time points used to determine the delay T_W between the transient and the first subsequent appearance of a slow wave. (B) T_W increases with the amplitude (labeled 'Transient F/F_0') of the previous Ca^{2+} transient. This Ca^{2+} transient amplitude in turn decreases with an increase in the mean cardiac Ca^{2+} load at rest (C). A 2nd order polynomial fit was used in B and C.

increased gradually after a perfusion period of 30 min. During this gradual transition from normal to elevated resting Ca^{2+} the dynamics of SCW's and the transients followed the relationships shown in Fig. 4C in that the amplitude of Ca^{2+} transients was inversely related to the resting Ca^{2+} level ($R = 0.55$, 37 myocytes). Therefore, myocytes with low resting Ca^{2+} and consequently, high amplitude Ca^{2+} transients were more effective in suppressing SCW's than low amplitude Ca^{2+} transients.

With increasing resting Ca^{2+} the slow waves became smaller in amplitude and eventually disappeared. Analysis of the velocity of SCW's revealed an inverse relationship between resting Ca^{2+} levels and propagation speed ($R = 0.72$, $N = 33$, Fig. 5), a finding that contradicts previous reports (see Discussion).

3.3. Propagation of Ca^{2+} waves between myocytes

In the majority of the observations, SCW's were confined to individual myocytes. The waves often reached the cell borders at high intensity values before they vanished. This observation suggested collision with cell borders without propagation into neighboring cells. In many cases however, an SCW crossed the cell border and propagated into a neighboring myocyte. This propagation could assume various characteristics. In the example in Fig. 6 a series of sequential images depicts two myocytes (outlined by the dashed orange lines). During the first 120 ms, an SCW was generated in the left cell (frames #1–3) while no visible Ca^{2+} changes were detected in the right cell. In frame #4, the SCW crossed the cell border from left to right, leading to a SCW in the other myocyte (arrow in frame #4). Both waves then gradually vanished (frames
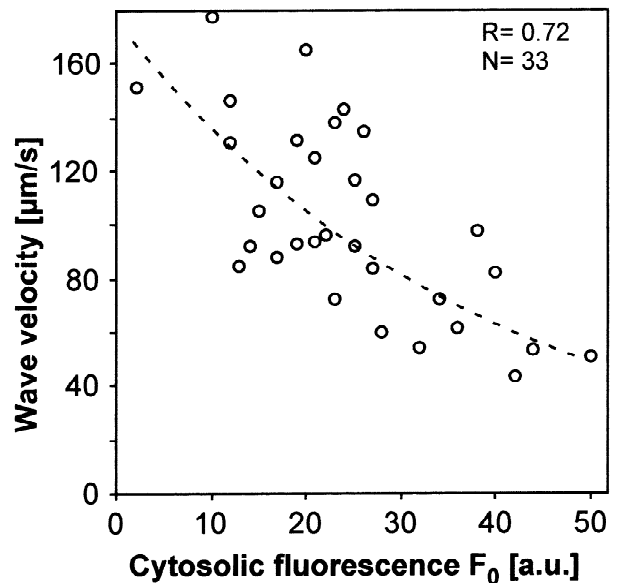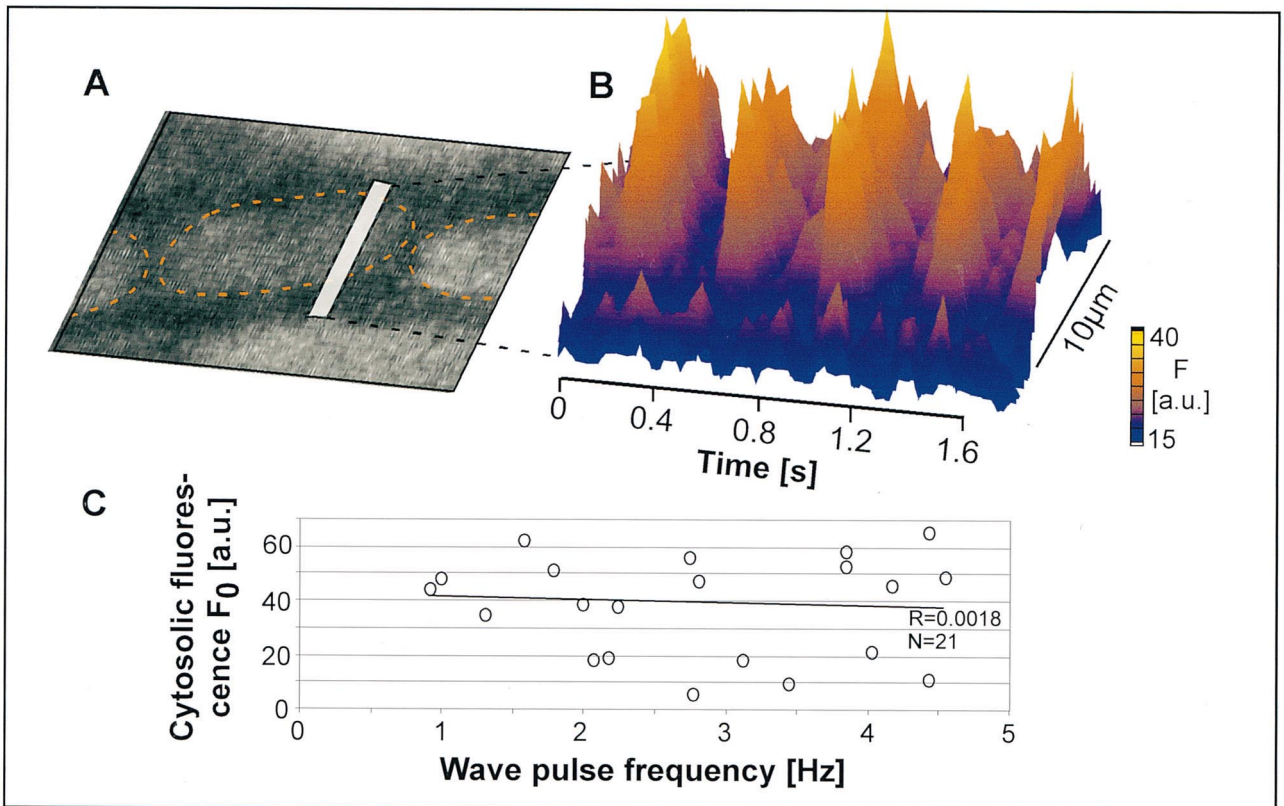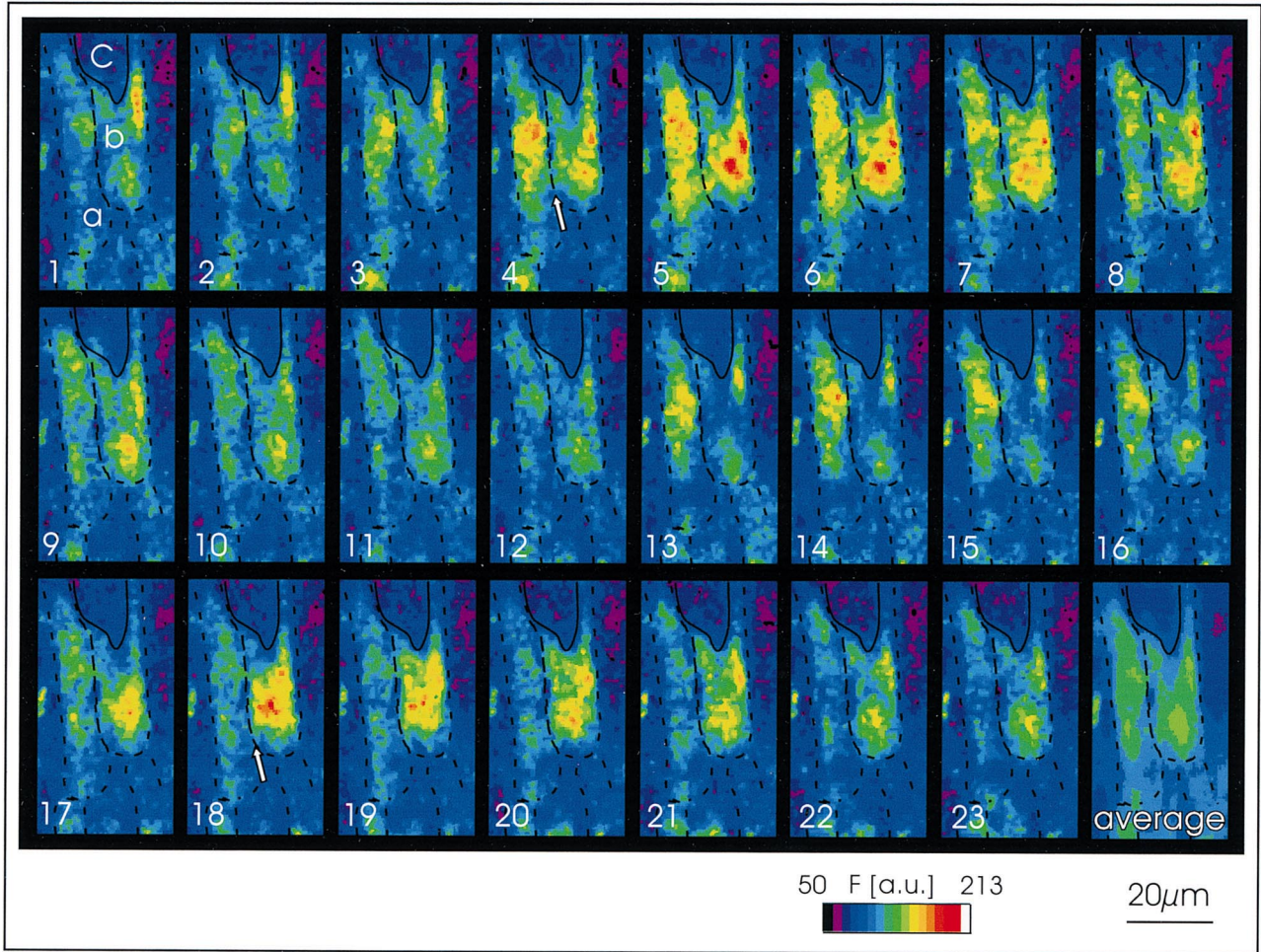

Fig. 5. Velocity of intracellular slow Ca^{2+} waves as a function of cytosolic Ca^{2+} load. In 33 cells the wave speed tended to increase with a decrease in cellular Ca^{2+} ($R = 0.72$, exponential fit).

50   F [a.u.]   213

20μm

10μm

40
F
[a.u.]
15

#7–12). Subsequently, a second smaller wave in the left cell (frames #13–19) did not reach the crossing point and hence did not induce Ca^{2+} changes in the right cell. Interestingly, an SCW in the right cell (frames #16–23) reached the contact point with high intensity (see arrow in frame #18) but did not propagate into the left cell. Thus, Ca^{2+} spread from a first into a second cell was not always followed by a spread in the opposite direction (unidirectional block).

3.4. Rhythmicity of slow Ca^{2+} waves

In most cases, SCW's were generated at random wave-to-wave intervals. However, distinct waves were occasionally recorded with a high degree of rhythmicity. This rhythmicity was always confined to one cell and apparently did not correspond to any activity in other cells nor was there ever any propagation into neighboring cells observed. The cell shown in Fig. 7A and B produced regular Ca^{2+} waves every 380 ± 9 ms (mean$\pm$S.D.). Fig. 7C shows a plot of the frequency of such highly rhythmic slow waves in 12 different preparations versus the cytosolic diastolic Ca^{2+} level of the respective myocytes. Interestingly, there was no correlation between frequency of this wave type and the Ca^{2+} loading.

3.5. Spatio-temporal occurrence of slow Ca^{2+} waves in the cellular network

SCW's lead to changes in transmembrane potential, that are supposed to trigger new propagated action potentials [20]. An arrhythmogenic effect of such local waves could be the consequence of both an increased local wave frequency and of the spatial frequency. The spatio-temporal occurrence of slow Ca^{2+} waves within an area of 150×120 μm is shown in Fig. 8. Within such a small region spatial electronic interaction of the changes in transmembrane potential induced by SCW's is likely to occur (see Discussion). Panel A shows the temporal occurrence of SCW's in one such limited area containing 39 myocytes during an interval of 4 s. The arrows indicate intercellular propagation of SCW's observed during the whole interval. In order to define the potential effect of temporal summation, the simultaneous occurrence of SCW's was assessed in 400 ms intervals during the 4

s-period. The black dots in Panel B denote the cells producing Ca^{2+} waves at the given time interval during the period. Panel C illustrates the results of four experiments with areas containing at average 31 ± 6 myocytes. Between 10 and 20% of cells produced SCW's at each determined instant within the recorded area of 150×120 μm.

4. Discussion

4.1. Relationship between Ca^{2+} transients and SCW's

Slow Ca waves (SCW's) were consistently observed *after* bursts of electrical stimulation. During normal stimulation rates SCW's were only observed in ischemic conditions (not shown). This indicates that normal electrical excitation suppressed SCW's and that, in general, the appearance of SCW's was associated with an elevation of cytosolic Ca^{2+}. Thus, our results are in accordance with previous studies describing the relation between cytosolic Ca^{2+} and propagating cytosolic SCW's [5,12]. The time interval between the last stimulated Ca^{2+} transient and the first appearance of a SCW was dependent on the resting Ca^{2+} level. A similar result was described in a recent study using freshly isolated guinea-pig myocytes [21] that showed that global Ca^{2+} transients lead to cytosolic suppression of local Ca^{2+} events. It was found that Ca^{2+} release from SR stores was required to induce this suppression. The duration of the suppression was reduced with an elevation of $[Ca^{2+}]_i$ and with an increase in Ca^{2+} SR contents (E. Niggli, personal communication).

4.2. Intracellular initiation and propagation of SCW's

In our experiments, the majority of Ca^{2+} waves originated intracellularly in an area corresponding to the center third of the cells and subsequently traveled to the periphery (Fig. 3). It was proposed that the initiation of SCW's is a consequence of a restricted, localized summation of individual Ca^{2+} sparks that reach a critical concentration level [2,4,22] and induce a propagated regenerative Ca^{2+} response. In our experiments, the location of the cell nucleus could explain a central initiation site. An interaction between cytosolic Ca^{2+} and nuclear Ca^{2+} has recently been reported in isolated myocytes [23]. The Ca^{2+} sparks per se, which were occasionally observed at the

---

Fig. 6. Intercellular uni-directional propagation of Ca^{2+} waves. Frame-by-frame recording (every 40 ms) of several myocytes (outlined by the black dotted lines). The last frame shows the average intensity distribution during this sequence. The wave front in the left cell (a) reaches the cell border, leading to a sudden Ca^{2+} increase in the right cell (b, arrow in frame #4). At the same contact point, a subsequent wave in the right cell does not spread into the left cell (arrow in frame #18). C=capillary.

Fig. 7. A. Ca^{2+} induced fluorescence changes recorded from the middle cell at the ROI indicated by a white field. B. Rhythmic pulsatory waves were observed as their wave fronts passed through the ROI shown in A. The wave pulse frequencies were in the range of 1–4.5 Hz, and were found to be independent from the intracellular Ca^{2+} load (C).
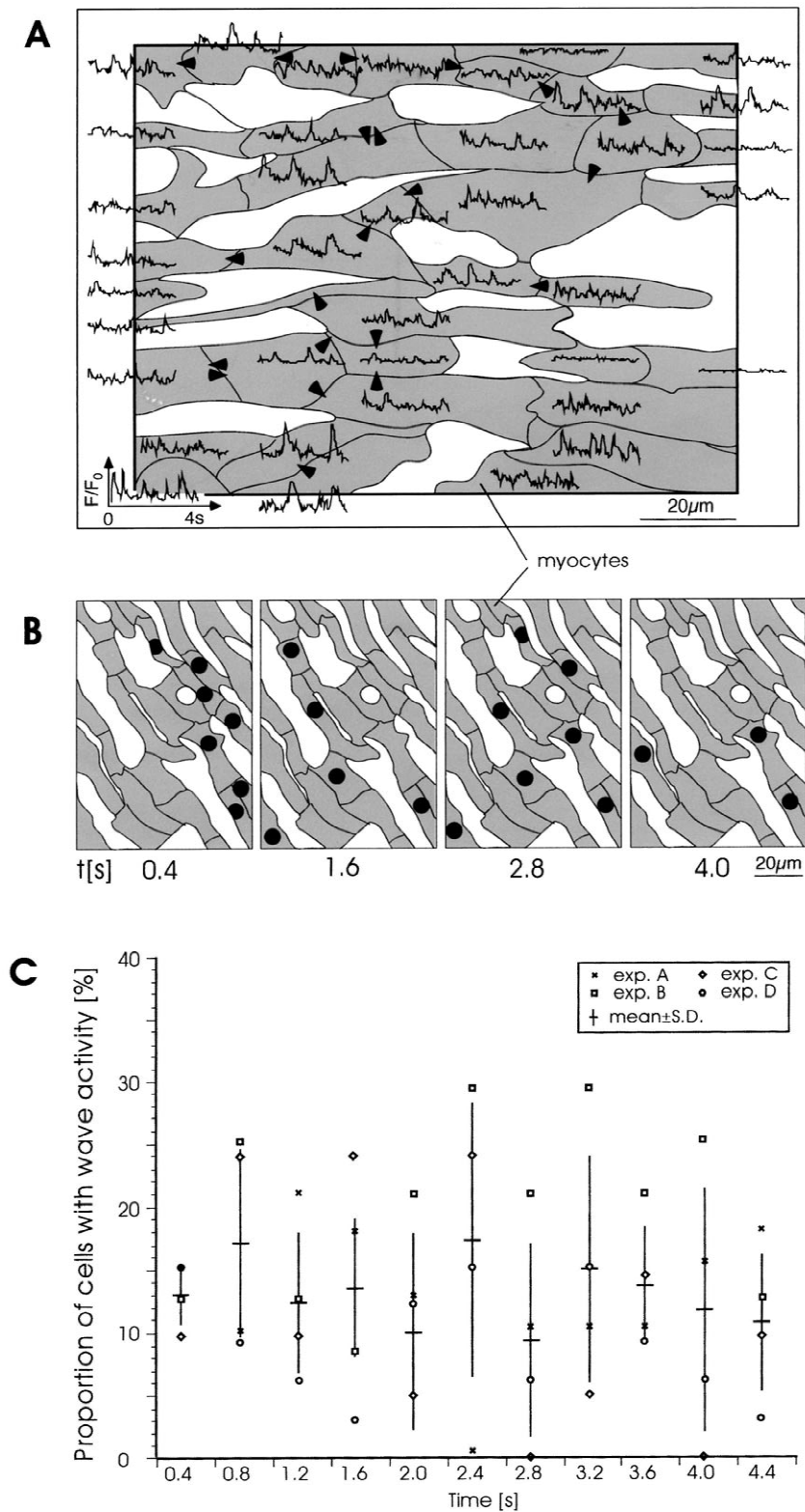
Fig. 8. Spatial distribution of Ca^{2+} waves. A. Reconstruction of a simultaneous recording of Ca^{2+} waves from a 120×150 μm ventricular segment during 4 s. Arrows indicate intercellular communication at any point during the 4 s-period. B. Four 400 ms-frames recorded every 1.2 s in another preparation. Black dots indicate the number of waves observed during the 400 ms-window in the respective myocytes. C. Percentage of myocytes exhibiting simultaneous slow Ca^{2+} waves during subsequent 400 ms-frames in arbitrary 120×150 μm square myocyte layers (four experiments).

limit of detection with our method (A. Baader, personal communication), occurred anywhere in the cytosol.

The intracellular propagation velocity of SCW's in our experiments was in the range of 50 to 180 μm/s. This is in agreement with previous studies that reported values of about 100 μm/s [5,12,24]. Although in our experiments the probability of SCW initiation increased with increasing $[Ca^{2+}]_i$, propagation velocity of individual waves decreased (Fig. 5). This contradicts previous reports showing an increase in propagation velocity with increase in cytosolic $[Ca^{2+}]$ [5,12]. The reason for this discrepancy, which appeared to be significant (Fig. 5), remains to be elucidated. It may be speculated that Ca^{2+} release from the SR or from the nucleus would produce a higher local Ca^{2+} concentration difference at lower $[Ca^{2+}]_i$ than at high cytosolic $[Ca^{2+}]$ loads. This $[Ca^{2+}]$ gradient may facilitate a higher propagation velocity of the induced SCW. Besides being a Ca^{2+} indicator, Fluo-3 has the side effect to buffer cytosolic Ca^{2+} to some degree. This might have affected our results in Figs. 4 and 5 with respect to the properties of both transients and SCW's. We have minimized this problem by keeping all loading parameters absolutely constant throughout our experiments.

In a recent study, slow Ca^{2+} waves were defined and named on the basis of their frequency [12]. Besides SCW's (3.8–28.1 waves/min $\approx$0.06–0.5 Hz) which were of the type also described in Figs. 2 and 3, these authors described a further type of Ca^{2+} wave (so-called 'agonal waves'), which were characterized by a high frequency (133.1 waves/min $\approx$2.2 Hz), a high degree of rhythmicity and an initiation at high cytosolic $[Ca^{2+}]_i$. In our experiments relatively frequent (1–5 Hz) and highly regular waves were also observed, in coexistence with the slower and relatively irregular waves. However, the frequency of these waves showed no dependency on the cytosolic $[Ca^{2+}]_i$. A further type of regular Ca^{2+} waves was described in isolated cardiac myocytes as a consequence of circus movements with re-entry around the cell nucleus serving as a fixed anatomical obstacle [25]. In our experiments such an intracellular circus movement was not observed.

4.3. Spatio-temporal occurrence of Ca^{2+} waves and potential relevance for arrhythmias

Delayed afterdepolarizations (DAD's) are generally thought to involve electrogenic Na/Ca exchange [26,27] and, possibly, chloride currents [28]. These mechanisms result from the transduction of a chemical Ca^{2+} wave into a change in electrical membrane potential. A propagated action potential is generated, if the change in membrane potential exceeds the threshold for Na^+ inward current. While this mechanism is undisputed at the level of the single cell, its generation in a network of coupled cells and in tissue seems more complex. This is because single cells

exhibiting SCW's and, probably DAD's, will be electrotonically influenced by neighboring cells. As in another initiation of focal mechanisms, a minimal amount of tissue needs to be activated in a coordinated manner for an excitatory effect [29]. As a major goal of this study, we therefore investigated the spatio-temporal interaction among various cells. Such interaction could be caused by (1) propagation of SCW's across cell borders, and/or (2) spatio-temporal coexistence of SCW's in closely adjacent cells exerting a mutual electrotonic influence.

Intercellular Ca^{2+} waves were observed that showed a clear spatial restriction to two, or at most three cells. At this very small scale, propagation phenomena such as collision with cell borders and unidirectional propagation occurred (Fig. 6). Also, the observed conflation of SCW's in one cell by waves from neighboring cells (Fig. 8) could represent a mechanism of synchronization. The reason of the consistent restriction of SCW's to only a few cells is not fully evident. Lamont et al. [10] interpret it as a useful mechanism to limit arrhythmic activity. It is known that Ca^{2+} per se and in conjunction with cellular acidification decreases gap junctional conductance [30,31]. Thus, Ca^{2+} increase might be a self-limiting factor for intercellular Ca^{2+} diffusion. However, the SCW's occurred concomitantly with fast Ca^{2+} transients and with coordinated visible mechanical activity, indicating that the electrical excitation process was not markedly slowed in presence of SCW's. This argument speaks against a major degree of cell-to-cell uncoupling during the occurrence of SCW's at slightly or moderately elevated cytosolic $[Ca^{2+}]_i$. Phenomena such as collision and extinction of SCW's were interpreted on the bases of 2-dimensional measurements in a given focal plane. It is likely that these phenomena were also affected by 3-dimensional propagation which was not assessed in our experiments.

Delayed afterdepolarizations in heart occur mostly as relatively fast and regular transient changes in membrane potential. Spatial as well as temporal summation (Fig. 8) could explain that SCW's, which as individual waves were rather slow (2–5 Hz), might lead to a relatively rapid electrical excitation. In the present experiments, we selected an area (150$\times$120 μm) with a diameter considerably smaller than the electrical space constant, to investigate the spatio-temporal occurrence of SCW's. Within this area 10–20% of the cells showed non-synchronized SCW's. Both spatial summation or inhibition might occur in such a case, and summation might lead to a higher overall frequency. However, the rhythmicity of DAD's observed in macroscopic tissue is not easily explained by the observed spatio-temporal occurrence of SCW's, because the slow Ca^{2+} waves were not phase-locked. This suggests that additional factors might determine whether localized SCW's lead to electrical excitation and arrhythmias.

In summary, our results show intercellular diffusion and a close spatio-temporal interaction of slow Ca^{2+} waves. Summation of such waves might explain the production

and the relatively high overall frequency of triggered action potentials. However, the exact mechanism of synchronization remains to be determined.

Acknowledgements

References

[1] Allen DG, Kurihara S. Calcium transients in mammalian ventricular muscle. Eur Heart J 1980:5–15.

[2] Cheng H, Lederer WJ, Cannell MB. Calcium sparks: elementary events underlying excitation–contraction coupling in heart muscle. Science 1993;262:740–744.

[3] Del Nido PJ, Glynn P, Buenaventura P, Salama G, Koretsky AP. Fluorescence measurement of calcium transients in perfused rabbit heart using rhod 2. Am J Physiol 1998;274:728–741.

[4] Wier WG, Ter Keurs HEDJ, Marban E, Gao WD, Balke CW. Ca^{2+} sparks and waves in intact ventricular muscle resolved by confocal imaging. Circ Res 1997;81:462–469.

[5] Minamikawa T, Cody SH, Williams DA. In situ visualization of spontaneous calcium waves within perfused whole rat heart by confocal imaging. Am J Physiol 1997;272:236–243.

[6] Miura M, Boyden PA, Ter Keurs HEDJ. Ca^{2+} waves during triggered propagated contractions in intact trabeculae. Am J Physiol 1998;274:266–276.

[7] Miura M, Boyden PA, Ter Keurs HE. Ca^{2+} waves during triggered propagated contractions in intact trabeculae. Determinants of the velocity of propagation. Circ Res 1999;84:1459–1468.

[8] Zhang YM, Miura M, Ter Keurs HE. Triggered propagated contractions in rat cardiac trabeculae. Inhibition by octanol and heptanol. Circ Res 1996;79:1077–1085.

[9] Ter Keurs HE, Zhang YM, Miura M. Damage-induced arrhythmias: reversal of excitation–contraction coupling. Cardiovasc Res 1998;40:444–455.

[10] Lamont C, Luther PW, Balke CW, Wier WG. Intercellular Ca^{2+} waves in rat heart muscle. J Physiol 1998;512:669–676.

[11] Hama T, Takahashi A, Ichihara A, Takamatsu T. Real time in situ confocal imaging of calcium wave in the perfused whole heart of the rat. Cell Signal 1998;10:331–337.

[12] Kaneko T, Tanaka H, Gyamada M, Kawata S, Takamatsu T. Three distinct types of Ca^{2+} waves in Langendorff-perfused rat heart revealed by real-time confocal microscopy. Circ Res 2000;86:1093–1099.

[13] Boyden P, Pu J, Pinto J, ter Keurs H. $Ca^{(2+)}$ transients and $Ca^{(2+)}$ waves in Purkinje cells: role in action potential initiation. Circ Res 2000;86:448–455.

[14] Fleischhauer J, Lehmann L, Kléber AG. Electrical resistances of interstitial and microvascular space as determinants of the extracellular electrical field and velocity of propagation in ventricular myocardium. Circulation 1995;92:587–594.

[15] Cascio WE, X YG-J, Kléber AG. Passive electrical properties, mechanical activity, and extracellular potassium in arterially perfused and ischemic rabbit ventricular muscle. Circ Res 1990;66:1461–1473.

[16] Cohen NM, Lederer WJ. Changes in the calcium current of rat heart ventricular myocytes during development. J Physiol 1988;406:115–146.

[17] Gomez JP, Potreau D, Raymond G. Intracellular calcium transients from newborn rat cardiomyocytes in primary culture. Cell Calcium 1994;15:265–275.

[18] Anversa P, Olivetti G, Loud AV. Morphometric study of early postnatal development in the left and right ventricular myocardium of the rat. I. Hypertrophy, hyperplasia, and binucleation of myocytes. Circ Res 1980;46:495–502.

[19] Takahashi A, Camacho P, Lechleiter JD, Herman B. Measurement of intracellular calcium. Physiol Rev 1999;79:1089–1125.

[20] Lakatta EG. Functional implications of spontaneous sarcoplasmatic reticulum Ca^{2+} release in the heart. Cardiovasc Res 1992;26:193–214.

[21] Del Principe F, Egger M, Niggli E. Calcium signalling in cardiac muscle: refractoriness revealed by coherent activation. Nature Cell Biol 1999;1:323–329.

[22] Cheng H, Lederer MR, Lederer WJ, Channell MB. Calcium sparks and $[Ca^{2+}]_i$ waves in cardiac myocytes. Am J Physiol 1996;270:148–159.

[23] Genka C, Ishida H, Ichimori K, Hirota Y, Tanaami T, Nakazawa H. Visualization of biphasic Ca^{2+} diffusion from cytosol to nucleus in contracting adult rat cardiac myocytes with an ultra-fast confocal imaging system. Cell Calcium 1999;25:199–208.

[24] Takamatsu T, Wier WG. Calcium waves in mammalian heart: quantification of origin, magnitude, waveform, and velocity. FASEB J 1990;4:1519–1525.

[25] Lipp P, Niggli E. Microscopic spiral waves reveal positive feedback in subcellular calcium signalling. Biophys J 1993;65:2272–2276.

[26] Kass RS, Tsien RW, Weingart R. Ionic basis of transient inward current induced by strophantidin in cardiac Purkinje fibres. J Physiol 1978;281:209–226.

[27] Niggli E, Lederer WJ. Activation of Na–Ca exchange current by photolysis of caged calcium. Biophys J 1993;65:882–891.

[28] Trafford AW, Diaz ME, Eisner DA. Ca-activated chloride current and Na–Ca exchange have different time courses during sarcoplasmic reticulum Ca release in ferret ventricular myocytes. Pflugers Archiv-Eur J Physiol 1998;435:743–746.

[29] Fozzard HA, Schoenberg M. Strength-duration curves in cardiac Purkinje fibres: effects of liminal length and charge distribution. J Physiol (Lond) 1972;226:593–618.

[30] Noma A, Tsuboi N. Dependence of junctional conductance on proton, calcium and magnesium ions in cardiac paired cells of guinea-pig. J Physiol 1987;382:193–211.

[31] Firek L, Weingart R. Modification of gap junction conductance by divalent cations and protons in neonatal rat heart cells. J Mol Cell Cardiol 1995;27:1633–1643.